Published by Nigerian Society of Physical Sciences. Hosted by FLAYOO Publishing House LTD

Recent Advances in Natural Sciences

Journal Homepage: https://flayoophl.com/journals/index.php/rans

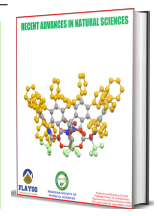

Geothermal parameter assessment in the Southwestern Sokoto Basin, Nigeria, using spectral analysis (centroid method)

U. Z. Magawata[a,*], N. K. Olasunkanmi[b], T. A. Issa[c]

[a]*Physics and Material Science Department, Kwara State University, Malete, Nigeria*
[b]*Physics Department Kebbi State University of Science and Technology, Aliero, Nigeria*
[c]*Department of Geology and Mineral Science, Kwara State University, Malete, Nigeria*

ARTICLE INFO

Article history:
Received: 26 January 2024
Received in revised form: 05 Feb. 2024
Accepted: 14 May 2024
Available online: 12 June 2024

Keywords: Geothermal parameters, Spectral analysis, Heat flow, Sokoto basin

DOI:10.61298/rans.2024.2.1.47

ABSTRACT

This study utilized spectral analysis (centroid method) to assess geothermal parameters in the southwestern part of the Sokoto Basin, Nigeria. The high-resolution airborne data comprised forty-nine (49) overlapping blocks, and each block was divided into 55x55 km to evaluate essential parameters such as depth to the top boundary (Z_t), centroid depth (Z_o), and magnetic source bottom ($Z_b = 2Z_o\text{-}Z_t$). The analysis revealed variable Curie points depths (CPD), ranging from 3.89 km to 26.56 km. The lowest CPD is primarily associated with basement rocks within anomalies A, B, C, D, E, F, G, H, and I, with an average CPD of 9.16 km. Furthermore, the thermal gradients ranged from 21.84 °C/km to 149.10 °C/km, with an average thermal gradient of 73.30 °C/km. The heat flow exhibited variations between 54.81 mW/m²and 374.24 mW/m², with average heat flow of 180.4 mW/m², indicating significant geothermal potential zones. The high thermal gradients and heat flow regions were identified, around anomalies A, B, and C. Additionally, temperature gradients identified at shallow depths ranged from 110 °C/km to 150 °C/km. The results reveal the presence of high-temperature points and anomalous geothermal potentials, particularly within anomalies A, B, and C, thus requiring further investigation for sustainable geothermal energy generation in the study area.

1. INTRODUCTION

Geothermal exploration naturally influences the regional and local structural setting [1]. This exploration hinges on crucial factors such as the Curie-depth point (CPD), temperature gradient, heat flow, and hydro-geological regions, all intimately linked to the geodynamic setting [2]. The Sokoto Basin, northwestern Nigeria, has recently garnered attention as a region with significant geothermal potential, with its unique geological characteristics and proximity to tectonic features [3].

The Nigeria sector of the basin is underlain to the east and south by Precambrian basement complex rock comprises igneous and metamorphic rocks, and to the north in the Tassaili and the Hoggar mountains by Cambrian beds [3]. The basin holds promising exploration and utilization of geothermal resources. The potential for geothermal energy in the Sokoto Basin resulted from several geological indicators, including sedimentary formations and associated thermal anomalies [3]. The sedimen-

*Corresponding Author Tel. No.: +234-703-4115-908.
e-mail: uzayyanu@yahoo.com (U. Z. Magawata)

tary rocks in the Sokoto Basin, such as the Gwandu Formation and the Dange Formation, are believed to host geothermal reservoirs. These formations exhibit thermal anomalies, suggesting subsurface heat flow and the possibility of geothermal activity. As the demand for sustainable energy sources grows, understanding and harnessing the geothermal potential of the Sokoto basin could play a crucial role in Nigeria's energy landscape. Previous research has highlighted the significance of depth to the bottom of magnetic sources (DBMS) while estimating CPDs, often occurring at approximately 580 °C [1, 2, 4]. These estimations are crucial in characterizing deformation modes, depth, and the Curie temperature distribution within the Earth's continental crust [4, 5]. Significantly, high temperature fluid movement can alter the magnetic properties of materials, rendering them paramagnetic [1].

Regional magnetic anomaly data can sometimes be employed to estimate depth rather than relying directly on temperature data [1]. Some studies conducted in different basins and geological areas on geothermal potentials emphasize the significance of CPD and DBMS in determining regional heat flow and crustal temperature, especially within sedimentary basins rich in organic matter maturity [1, 2, 6–22]. Regional geothermal studies within the Sokoto Basin show that the sedimentary thicknesses were range between 1.0 to 2.7 km, statistically equivalent to DBMS or basement depths [23–25]. The heat flow variation using the bottom-hole temperature measurements from the entire Sokoto basin ranged between 20.58 ^{0}C/km to 51.02 ^{0}C/km with average temperature gradient of 33.99 ^{0}C/km [26]. Also, according to Taufiq *et al*. [23] reports thermal gradient of the Sokoto basin ranges between 46.4 ^{0}C/km to 116.9 ^{0}C/km, with mean values equivalent to the 81.6 ^{0}C/km.

This study uses a spectral centroid approach to estimate CPD from geothermal parameters using a high-resolution airborne dataset. However, it provides valuable insights into the most promising geothermal exploration areas, paving the way for sustainable energy generation within the region.

2. GEOLOGICAL SETTING OF THE AREA

The study area is situated in the southwestern part of the Sokoto Basin in Northwestern Nigeria, bounded by coordinates 3.50N to 5.50N and 10.00E to 12.00E, covering an area of approximately 48,400 km^2. The Sokoto (Iullemmeden) Basin in south-central Saharan Africa is circular intra-cratonic and spans about 700,000 km^2 and is a circular intra-cratonic basin in south-central Saharan Africa. It traverses regions of northwestern Nigeria and parts of the Republics of Benin, Mali, and Niger [27]. The region is part of the late Proterozoic–early Phanerozoic of the Sokoto sector, effectively demarcating the West African craton [3]. The tertiary marine deposits within the Sokoto Basin comprise red, mottled massive clays with intermittent sandstone intercalations. These sediments correspond to the Gwandu Formation of Northern Nigeria and are discordantly overlain by a substantial series of deposits. These deposits consist of massive white clays interspersed with red mudstones, sandstones of varying grain sizes, and occasional peat bands [28]. The geological composition of the study area is shown in Figure 1 and it includes a diverse range of rock types, such as metaconglomerate, sandstone, ironstone, laterites, quartz-mica schist, clay materials, banded granite, biotite, migmatite, gneiss, biotite-hornblende, medium coarse-grained diorite, and others. These rock types collectively contribute to the geological complexity of the area. The study area's geological features are closely associated with brittle and ductile fault structures and planes of schistosity that intersect various rock types, including phyllites, schists, quartzites, gneisses, and granitoid masses in proximity. These geological characteristics link two regional fault systems [21, 29, 30].

3. MAGNETIC DATA PROCESSING AND ANALYSIS

Sixteen gridded sheets of high-resolution aeromagnetic data from the Nigeria Geological Survey Agency (NGSA) were obtained. These datasets were acquired by Fugro Aero Services Ltd. between 2004 and 2009 for mineral resource development in Nigeria [31]. The data were collected along 500 m line spacing in the NW-SE direction, maintaining an 80 m clearance survey lines, and tie lines were spaced at 2000 m intervals in the NE-SW direction. Corrections were applied for diurnal variation and the International Geomagnetic Reference Field (IGRF) to ensure data accuracy. The magnetic inclination (I) of I= 3.021 and declination (D) of D = -0.245 were measured, respectively. Figure 2a show the composite 'RMA' map was divided into 49 overlapping square blocks, each covering an area of 55x55 km square. To enhance the magnetic anomalies' contrast, reduction-to-equator residual magnetic anomaly ('RTE-RM') technique was employed as shown in Figure 2b which is consistent with Akinlalu *et al*. [32] and contributes to the symmetrical representation of anomalies concerning their sources, facilitating contour delineation [33, 34]. The source parameter imaging (SPI), also known as local wave numbers, is used to estimate depth equation (1) as developed by Finn and Ravat [35]. The source parameter imaging 'SPI' or the local wave numbers developed by Finn & Ravat [35], and is computed for depth estimate as seen in equation (1),

$$K = \frac{\frac{\partial^2 M \partial M}{dxdzdx} - \frac{\partial^2 M \partial M}{dx^2 dz}}{(\frac{\partial M}{dx})^2 + (\frac{\partial M}{dz})^2}, \tag{1}$$

where, M= magnetic field value, x= grid of the horizontal derivative in the x-direction, z= grid of the horizontal derivative in the x-direction, K= represent the peak value of located over the step source.

$$Depth = (x = 0)\frac{1}{K\,\max}. \tag{2}$$

A graph displaying the spectrum against the wave number (Rad/km) is employed to determine the Curie Point Depth (CPD) for each block.

3.1. CENTROID APPROACH

The centroid approach calculates the CPD [2, 5, 15, 34]. Other methods include the scaling spectrum methods [6], spectral peak method [34], forward modeling of the spectral peak method [35], and correlation between magnetic source depth and magnetic anomalies spectrum [2, 34]. According to Elkhateeb and Abdellatif [15], the density of the power spectrum of the magnetic field observed ($\varphi\Delta$T = (Kx, Ky) is given by

$$p(Kx, Ky) = \varphi m(Kx, Ky) \times F(Kx, Ky), \tag{3}$$

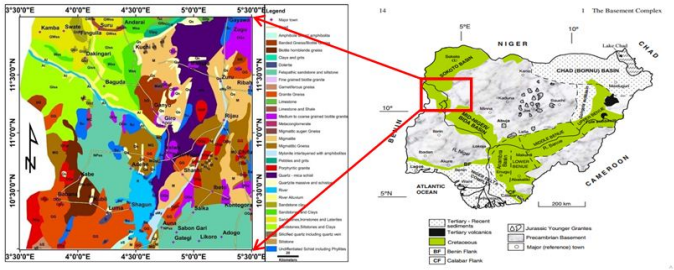

Figure 1. Geological map of the entire southwestern part of Sokoto basin, showing the representative rocks distribution of the basin modified after Rajagopalan [31], inset of the geological map of Nigeria.

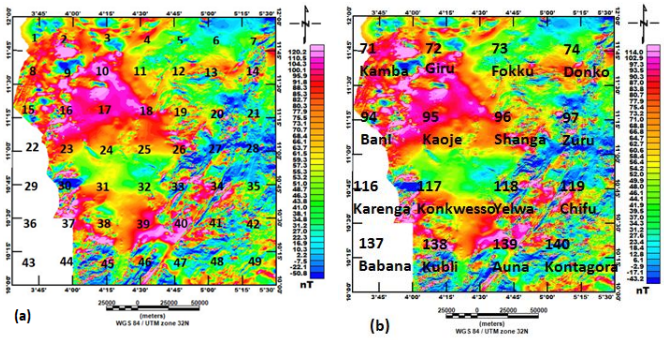

Figure 2. (a) Residual magnetic anomaly (RMA) showing block numbers, (b) Reduced to magnetic equator (RTE-RMA) map showing the aeromagnetic sheet numbers.

$$F(Kx, Ky) = 4\pi^2 C^2 m\phi(kx, ky)\ |m|^2\ |F|^2\ e^{-2|k|Zt} \times (1 - e^{-|k|(Zb-Zt)})^2, \quad (4)$$

where Cm^2 = constant quantity, φm = power spectrum magnetization, and (kx, ky) are wave numbers in the "x, y" directions. Magnetization factors are denoted by $|\Theta m|^2$, and magnetic field directions are represented by $\Theta f|^2$, respectively. Moreover, the top and the bottom magnetic layers are Z_t and Z_b, respectively. The x and y represent the random function while M(x, y) is random magnetization, and the constant values are m (kx, ky). The radially average power spectrum [36] is given by;

$$p(k) = A_1^{-2|k|Zt}(1 - e^{-2|k|(Z_b - Z_t)}), \quad (5)$$

where k is the wave number and A is constant

The power spectrum derives from a magnetic resource's central depth generated from a low wave number.

$$\ln(\frac{p(k)^2}{k}) = A2\,|k|\,Zo, \quad (6)$$

$$\ln(p(k)^2) = A3 - |2k|\,Zt, \quad (7)$$

where A2 and A3 are constant values, while P is the power spectral density, and the bottom depth can be determined as follows [2].

$$Z_b = 2Zo - Zt, \quad (8)$$

Additionally, equation (9) shows the links between heat flow and geothermal gradient using Fourier's law [36, 37].

$$q = k\frac{\partial T}{\partial z}, \quad (9)$$

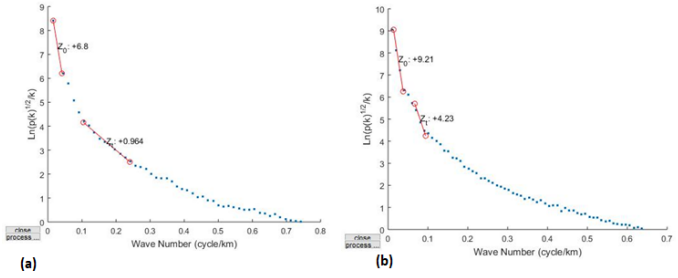

Figure 3. Radially averaged powered spectrum representative of (a) block 6 and (b) block 18 respectively.

where q = Heat flow (W/m^2), k = thermal conductivity ($Wm^{-1}K^{-1}$) and T = inducing filed (V/m). The Curie temperature is expressed as;

$$\theta c = (\frac{\partial T}{\partial Z})zb, \quad (10)$$

where Zb= is the basal depth or is called Curie point depth.

4. RESULTS AND DISCUSSION

4.1. CURIE DEPTH POINT (CDP) ESTIMATION

The power spectrum plots for blocks 6 and 18 in the southwestern part of the Sokoto basin were selected to represent the 49 blocks. These blocks' estimated depths to the top boundary (Z_t) were 0.964 km for block 6 and 4.23 km for block 18. Additionally, the centroid depth (Z_o) is estimated to be 6.8 km for block 6 and 9.21 km for block 18 in Figure 3a and 3b.

The visual examination of the depth to the bottom of the magnetic sources (DBMS) map as shown in Figure 4a reveals distinct regions of varying depths. Shallow and dipper depths, ranging from 85 m to 103.4 m, are associated with anomalies A, B, C, D, E, F, G, H, and I correspond to metasedimentary and basement rocks, with CPD values <9 km trending the SE part of the study area in Figure 4b. In contrast, the regions represent thick sedimentary or deep-lying magnetic source depths corresponding to anomalies O and P, trend the NW region with corresponding depths ranging from 465.2 to 754 m. According to Tanaka *et al*. and Salk *et al*. [2, 38], the shallow nature of CPDs and elated geodynamic environment commonly associated with plate boundaries, they report that the CPDs are less than 10 km. However, the sallow nature of the CPDs, around the mentioned anomalies attributed to high heat conductivity and the presence of igneous rocks.

The CPD observed from 15 to 25 km is due to island arcs and ridges. However, a CPD greater than 20 km indicates trenches and plateaus. In Figure 4b, the SE trends indicate a shallow CPD portion <15 km located within the basement complex rocks. The NW part of the study area revealed different CPD <27 km located particularly within anomaly O and P within the sedimentary basin and is consistent with the work of Nwankwo and Shehu [26]. However, the average CPD in the study area was 9.16 km. These findings align with a previous study by Shehu *et al*. [24], who evaluated the geothermal parameters of the entire Sokoto Basin, Nigeria, reporting a CPD of 27.83 km. Taufiq *et al*. [23] determined (CPD) values across the Sokoto basin using spectral analysis (centroid approach).

Table 1. Calculated geothermal parameters.

Spectral Blocks	Locations	Longitude (degree)	Latitude (degree)	Centroid depth Z_o (km)	Top boundary depth Z_t (km)	Curie point depth Z_b (km)	Geothermal gradient (^{o}C/km)	Heat flow (mW/m^2
1	North-west	3.75	11.75	5.93	1.51	10.35	56.04	140.66
2	North-west	4.00	11.75	4.7	1.27	8.13	71.34	179.07
3	North-west	4.25	11.75	4.91	1.64	8.18	70.90	177.97
4	North-east	4.50	11.75	4.77	1.31	8.23	70.47	176.89
5	North-east	4.75	11.75	4.03	1.67	6.39	90.77	227.82
6	North-east	5.00	11.75	6.8	0.964	12.64	45.90	115.21
7	North-east	5.25	11.75	5.44	1.52	9.36	61.97	155.53
8	North-west	3.75	11.50	8.6	1.79	15.41	37.64	94.47
9	North-west	4.00	11.50	8.04	1.78	14.30	40.56	101.80
10	North-west	4.25	11.50	5.29	1.95	8.63	67.21	168.69
11	North-east	4.50	11.50	5.52	2.15	8.89	65.24	163.76
12	North-east	4.75	11.50	4.18	2.19	6.17	94.00	235.95
13	North-east	5.00	11.50	4.59	2.5	6.68	86.83	217.93
14	North-east	5.25	11.50	5.35	2.01	8.69	66.74	167.53
15	North-west	3.75	11.38	14.4	2.24	26.56	21.84	54.81
16	North-west	4.00	11.38	8.75	2.81	14.69	39.48	99.10
17	North-west	4.25	11.38	7.51	2.81	12.21	47.50	119.23
18	North-east	4.50	11.38	9.21	4.23	14.19	40.87	102.59
19	North-east	4.75	11.38	5.68	2.86	8.50	68.24	171.27
20	North-east	5.00	11.38	5.32	2.64	8.00	72.50	181.98
21	North-east	5.25	11.38	3.92	2.84	5.00	116.00	291.16
22	North-west	3.75	11.00	4.92	2.11	7.73	75.03	188.33
23	North-west	4.00	11.00	7.69	1.62	13.76	42.15	105.80
24	North-west	4.25	11.00	6.24	2.18	10.30	56.31	141.34
25	North-east	4.50	11.00	5.78	2.17	9.39	61.77	155.04
26	North-east	4.75	11.00	3.88	1.48	6.28	92.36	231.82
27	North-east	5.00	11.00	4.01	1.57	6.45	89.92	225.71
28	North-east	5.25	11.00	4.03	1.35	6.71	86.44	216.96
29	South-west	3.75	10.75	7.94	1.71	14.17	40.93	102.74
30	South-west	4.00	10.75	7.7	1.88	13.52	42.90	107.68
31	South-west	4.25	10.75	4.24	1.4	7.08	81.92	205.62
32	South-east	4.50	10.75	4.44	2.01	6.87	84.43	211.91
33	South-east	4.75	10.75	3.62	1.48	5.76	100.69	252.74
34	South-east	5.00	10.75	2.49	1.07	3.91	148.34	372.33
35	South-east	5.25	10.75	2.6	1.31	3.89	149.10	374.24
36	South-west	3.75	10.50	5.99	1.79	10.19	56.92	142.87
37	South-west	4.00	10.50	4.69	1.92	7.46	77.75	195.15
38	South-west	4.25	10.50	4.86	1.59	8.13	71.34	179.07
39	South-east	4.50	10.50	3.62	1.09	6.15	94.31	236.72
40	South-east	4.75	10.50	3.51	1.17	5.85	99.15	248.85
41	South-east	5.00	10.50	4.03	1.02	7.04	82.39	206.79
42	South-east	5.25	10.50	4.9	1.11	8.69	66.74	167.53
44	South-west	3.75	10.25	5.29	1.3	9.28	62.50	156.88
45	South-west	4.00	10.25	3.42	1.31	5.53	104.88	263.25
46	South-east	4.25	10.25	3.37	1.67	5.07	114.40	287.14
47	South-east	4.50	10.25	3.8	1.95	5.65	102.65	257.66
48	South-east	4.75	10.25	4.9	1.54	8.26	70.22	176.25
49	South-east	5.00	10.25	9.15	1.33	16.97	34.18	85.79

The reported CPD values range from 5.96 km to 74.29 km, with an average value of 18.99 km. Shallow CPDs, similar to high geothermal parameters (heat flow and thermal gradient), are associated with anomalies A, B, and C. These anomalies agree

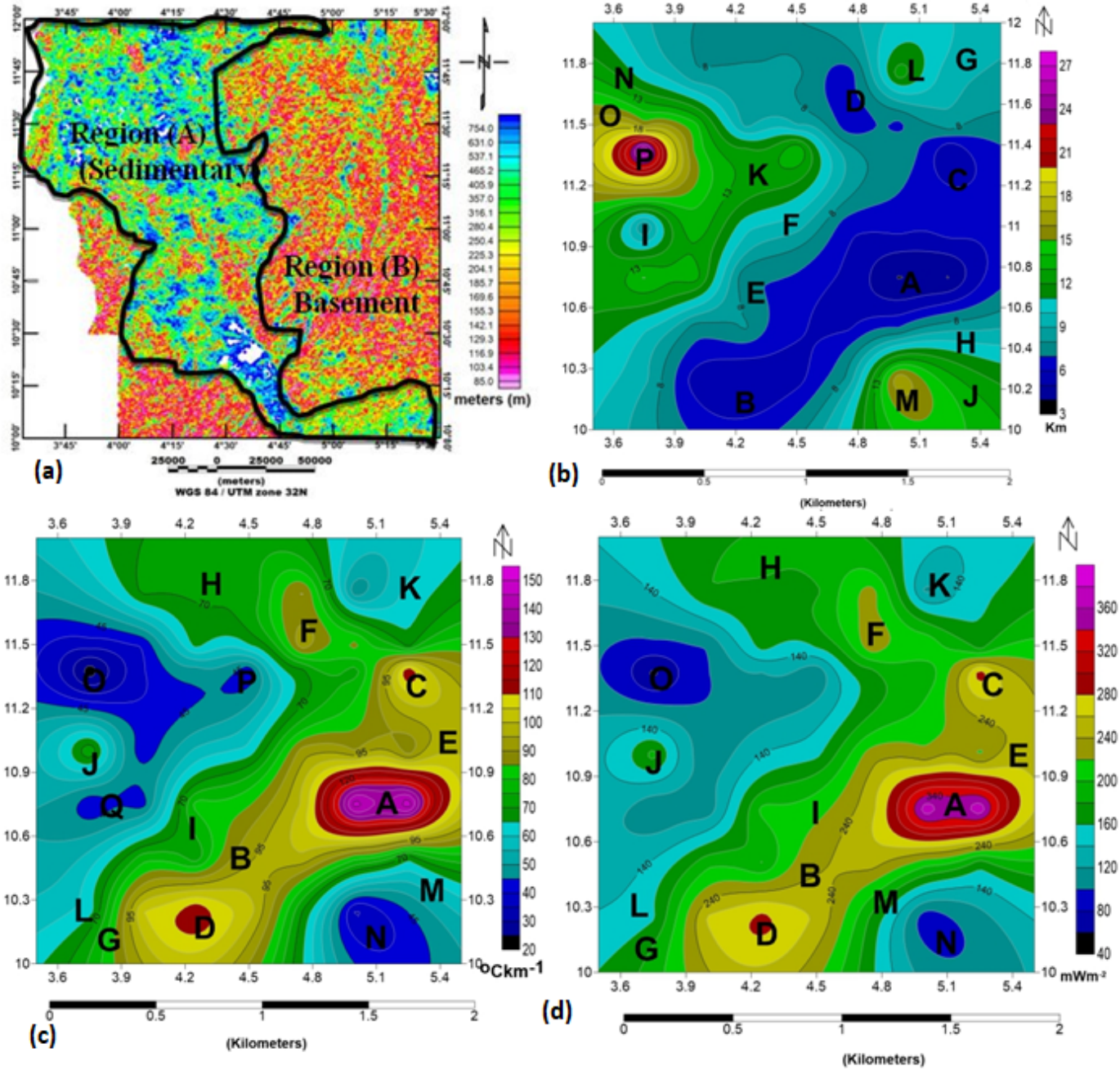

Figure 4. Map of the study area showing (a) Source parameter imaging (SPI) (b) Curie point depth (CPD) (c) Temperature gradient, and (d) Heat flow.

with the basement complex structure in the area, which strongly influences Pan-African granitic intrusions and the presence of tertiary basalt rocks. The study also identified a minimum thermal gradient value of 21.84 °C/km in block 15, contrasting with a maximum thermal gradient of 149.10 °C/km in block 35.

4.2. THERMAL GRADIENT AND HEAT FLOW VARIATION

Table 1 also reveals thermal gradients of the area varies between 21.84 °C/km to 149.0 °C/km, with an average thermal gradient of 73.30 °C/km. However, the areas with lowest thermal gradient include anomalies (N, O, P, Q, K, L, and M), while the moderate thermal anomalies includes (F, G, H, I, and J) located in the NW region of the study area and upper Bidda basin dominating the sedimentary strata as in Figure 4c. The lowest thermal gradient anomalies in a region attributed to a complex interplay of geological factors, including the composition of the Earth crust, tectonic processes, and heat flow variability.

The geological setting, such as the prevalence of sedimentary rocks with lower thermal conductivity, can contribute to a shallower thermal gradient. Tectonic activity, such as the absence of significant faulting or volcanic processes, reduced heat flow. Crustal thickness, lithospheric processes, and the distribution of heat-producing elements, such as uranium and thorium influence the thermal structure. Regions with high thermal gradient in-

cludes anomalies (A, B, C, D, and E) with thermal gradient values ranging from (110 ^{0}C/km to 150 ^{0}C/km) trending the SE part occupying the basement rocks formation. Those regions have significant geothermal signatures such as granitic intrusions (hydrothermal alteration can occur in the vicinity of granitic intrusions, leading to the formation of minerals like sericite, quartz, and sulfides) and Fault Zones, can provide pathways for geothermal fluids to migrate through the Earth crust. Mineral associated with fault zones may indicate the effects of hydrothermal alteration along these pathways. However, specific minerals within certain rock formations are one aspect of understanding the complex nature of geothermal systems.

High heat flows >80 mW/m^{-2} reported to exist in the basin [13, 23, 25, 26]. This suggest anomalous geothermal conditions. The heat flow within the study area ranges from 54.81 mW/m^2 to 374.24 mW/m^2 with an average heat flow of 180.40 mW/m^2 in Table 1. However, equation (9) indicates the links between heat flow and geothermal gradient through the Fourier's law. By considering a Curie temperature of 580 °C for magnetite and a thermal conductivity of K= 2.5 Wm^{-1} ^{0}C^{-1} for igneous rocks, the heat flow map in Figure 4d notices anomalies N, O, L, K, and M that represent the zones with minimum heat flow within the sedimentary basin part of the study area.

The thermal gradient is the rate at which temperature changes with depth and reduced heat flow as temperature differences drive heat transfer. If the geothermal gradient (change in temperature with depth) is shallow, it can contribute to lower heat flow from the Earth interior to the surface. However, Sedimentary basins with low heat flow may have limitated in petroleum and natural gas production. The thermal maturation of organic matter to hydrocarbons is influenced by heat. In contrast, anomalies H, I, G, J, E, and F exhibit low thermal anomalies with temperatures ranging from 40 °C/km to 80 °C/km, mainly within sedimentary strata. The areas with high heat flow values agrees with volcanic activities and metamorphism, meanwhile, high heat flow may also result from deep magmatic mass in association with young volcanism and faulted structure [38]. However, geological information significantly influences heat flow patterns within the study area. The high heat flow regions are primarily associated with igneous and metamorphic rocks.

In thermally continental regions, the estimated minimum heat flow for considerable geothermal energy generation is 60 mW/m^2 and the heat flow range from 80 to 100 mW/m^2 indicates probable anomalous geothermal conditions. The anomalously high heat flow values around 360 mW/m^2 were noticed, particularly in the metamorphic region of the study area, correlating with high thermal gradients >150 mW/m^2. However, the zone characterized by high thermal conductivity and has undergone complex geological processes over millions of years, including tectonic activities associated with the movement of Earth plates. The tectonic activity plays a substantial role in heat flow variations in the region and resulted in faulting, folding, and other structural deformations [2, 29, 39]. Zone with high CPD values coincide with low thermal gradients. In geothermal exploration, the CPD and thermal gradients are significant parameters that provide insights into the temperature distribution within the Earth crust.

5. CONCLUSION

This study utilizes high-resolution aeromagnetic data to unveil substantial geothermal potential in the southwestern part of Sokoto Basin Nigeria. It identifies CPD zones, with deeper zones corresponding to sedimentary areas and shallow zones corresponding to metamorphic or igneous regions, each linked to distinct structural trends. CPDs range from 3.89 km to 26.56 km, averaging 9.16 km. The lowest CPD zones values of 3.89 km and high thermal gradients indicate promising geothermal prospects. The thermal gradient varies from 21.8 °C/km to 149 °C/km, averaging 73.3 °C/km, suggesting favorable geothermal conditions. Heat flow ranges between 54.81 mW/m^2 and 374.24 mW/m^2, with an average exceeding 100 mW/m^2, signifying an anomalous geothermal state as per sedimentary thickness ranges from 0.964 km to 4.23 km, thus corroborate with geological information of the study area. These findings emphasize the need for further investigations within the Pan-African province to harness the region's geothermal energy resources.

References

[1] A.R. Bansal, G. Gabriel, V.P. Dimri & C.M. Krawczyk, "Estimation of depth to the bottom of magnetic sources by a modified centroid method for fractal distribution of sources: an application to aeromagnetic data in Germany", Geophysics **76** (2011) L11. https://doi.org/10.1190/1.3560017.

[2] A.Y. Tanaka, Y. Okubo & O. Matsubayashi, "Curie point depth based on spectrum analysis of the magnetic anomaly data in East and Southeast Asia", Tectono physics **306** (1999) 461. https://api.semanticscholar.org/CorpusID:129434570.

[3] J. B. Wright, D. Hastings, W. B. Jones & H. R. Williams, *Geology and mineralresources of West Africa*, George Allen and Urwin, London, 1985, pp. 90 – 120. https://doi.org/10.1007/978-94-015-3932-6.

[4] D. Ravat, A. Pignatelli, I. Nicolosi & M. Chiappini, "A study of spectral methods of estimating the depth to the bottom of magnetic sources from near-surface magnetic anomaly data", Geophysics J. Int. **169** (2007) 421. https://doi.org/10.1111/j.1365-246X.2007.03305.x.

[5] W. R. Roest, V. Verhoef & M. Pilkington, "Magnetic interpretation using the 3-D analytic signal", Geophysics **57** (1992) 116. https://doi.org/10.1190/1.1443174.

[6] S. Maus, D. Gordon & J. D. Fairhead, "Curie temperature depth estimation using a self similar magnetization model", Geophysical Journal International **129** (1997) 163. https://doi.org/10.1111/j.1365-246X.1997.tb00945.x.

[7] H. E.Ross, R. J. Blakely & M. D. Zoback, "Testing the use of aeromagnetic data for the determination of Curie depth in California", Geophysics **71** (2006) L51. https://doi.org/10.1190/1.2335572.

[8] G. Gabriel, I. Dressel, D. Vogel & C. M. Krawczyk, "Depths to the bottom of magnetic sources and geothermal prospectivity in Southern Germany", First Break **30** (2012) 39. http://dx.doi.org/10.3997/1365-2397.2012001.

[9] S. Saleh, M. Salk & O. Pamukcu, "Estimating Curie point depth and heat flow map for Northern Red Sea rift of Egypt and its surroundings, from aeromagnetic data", Pure and Applied Geophysics **170** (2013) 85. http://dx.doi.org/10.1007/s00024-012-0461-0.

[10] A. R. Bansal, S. P. Anand, M. Rajaram, V. K. Rao & V. P. Dimri, "Depth to the bottom of magnetic sources (DBMS) from aeromagnetic data of central India using modified centroid method for fractal distribution of sources", Tectono physics 603 (2013) 155. https://doi.org/10.1016/j.tecto.2013.05.024.

[11] S.N.P. Guimarães, V. M. Hamza & D. Ravat, *Curie depths using combined analysis of centroid and matched filtering methods in inferring thermomagnetic characteristics of Central Brazil*, 13th International Congress of the Brazilian Geophysical Society, Riode Janeiro, Brazil, 2013, pp. 26–29. https://doi.org/10.1190/sbgf2013-381.

[12] G. E. Obande & K. M. Lawal, L. A. Ahmed, "Spectral analysis of aeromagnetic data for geothermal investigation of Wikki Warm spring north-east Nigeria", Geothermic **50** (2014) 85. https://doi.org/10.1016/j.geothermics.2013.08.002.

[13] L. I. Nwankwo, "Estimation of depths to the bottom of magnetic sources and ensuing geothermal parameters from aeromagnetic data of upper

Sokoto Basin, Nigeria", Geothermics 54 (2015) 76. http://dx.doi.org/10.1016/j.geothermics.2014.12.00.

[14] R. Bello, C. Ofoha & N. Wehiuzo, ‘‘Geothermal gradient, Curie point depth and heat flow determination of some parts of lower Benue trough and Anambra basin, Nigeria, using high resolution aeromagnetic data", Phys. Sci. Int. Journal **15** (2017) 1. https://doi.org/10.4314/jasem.v25i10.10.

[15] S. O. Elkhateeb & M.A.G Abdellatif, ‘‘Delineation potential gold mineralization zones in a part of central eastern desert, Egypt using airborne magnetic and radiometric data", NRIAG J Astron Geophysics. **7** (2018) 361. https://doi.org/10.1016/j.nrjag.2018.05.010.

[16] J.A. Mono, T. Ndougsa-Mbarga, Y. Tarek, D.J. Ngoh & O.U.I.O. Amougou ‘‘Estimation of curie point depths, geothermal gradients and near-surface heat flow from spectral analysis of aeromagnetic data in the Loum-Minta area (Centre-East Cameroon)", Egyptian Journal of Petroleum **27** (2018) 1291. https://doi.org/10.1016/j.ejpe.2018.07.002.

[17] Y. Abubakar, S. Lim Hwee & A. A. Ismail, ‘‘Curie-point depths, geothermal gradients and sub-surface heat flow estimation from spectral analysis of high-resolution aeromagnetic data over Gongola basin and its environs, Northeastern Nigeria", Sains Malaysiana **51** (2022) 657. http://doi.org/10.17576/jsm-2022-5103-03.

[18] M. B. Yakubu, K. M. Lawal, B. B. M. Dewu & A. E. Ikpokonte, ‘‘Investigation of geothermal energy resource potential using the aero-magnetic and aero-radiometric data of Kano, Nigeria", Fudma journal of sciences **6** (2022) 296. https://doi.org/10.33003/fjs-2022-0601-900.

[19] K. Ewa & S. Kryrowska, ‘‘Geothermal exploration in Nigeria", Proceedings world geothermal congress. Zaria, Nigeria", (2010) 25. https://www.geothermal-energy.org/pdf/IGAstandard/WGC/2010/1152.pdf.

[20] T. O. Lawal & L. I. Nwankwo, ‘‘Evaluation of the depth to the bottom of magnetic sources and heat flow from high resolution aeromagnetic (HRAM) data of part of Nigeria sector of chad basin", Arabian J. Geosciences **10** (2017) 1. http://dx.doi.org/10.1007/s12517-017-3154-2.

[21] T. O. Lawal, L. I. Nwankwo, A. A. Iwa, J. A. Sunday & M. M. Orosun, ‘‘Geothermal energy potential of the Chad basin, north-eastern Nigeria", Journal of Applied Sciences and Environmental Management **22** (2018) 1817. https://www.ajol.info/index.php/jasem.

[22] B. E. Ikumbur, ‘‘The correlation of geothermal energy potential deduced from aeromagnetic and aeroradiometric data of Akiri and environs, North-Central Nigeria", Nigerian Society of Physical Sciences **1** (2023) 5. https://flayoophl.com/journals/index.php/rans.

[23] S. Taufiq, F. N. Okeke & D. N. Obiora ‘‘Assessment of geothermal potential of parts of Sokoto Basin, Northwest Nigeria using aero-radiometric data", Model Earth Syst. Environ **7** (2021) 1217. https://doi.org/10.1007/s40808-020-01013-3.

[24] A. T. Shehu, E. E. Udensi, J. O. Adeniyi & S. A. Jonah, ‘‘Spectral analysis of the magnetic residual anomalies over the Upper Sokoto Basin, Nigeria", Zuma J. Pure Appl. **6** (2021) 37. https://www.researchgate.net/publication/355163911_Spectral_analysis_of_the_magnetic_residual_anomalies_over_the_Upper_Sokoto_Basin_Nigeria.

[25] A. A. Adetona, E. E. Udensi & G. A. Agelaga, ‘‘Determination of depth to buried rocks under the lower Sokoto Basin, Nigeria using aeromagnetic data", Nigeria J. Phys. **19** (2007) 275. https://doi.org/10.4314/njphy.v19i2.38144.

[26] L. I. Nwankwo & A. T. Shehu, ‘‘Evaluation of curie-point depths, geothermal gradients and near-surface heat flow from high-resolution aeromagnetic (HRAM) data of the entire Sokoto Basin, Nigeria", Journal of Volcanology and Geothermal Research **305** (2015) 45. https://doi.org/10.1016/j.jvolgeores.2015.09.017.

[27] N. G. Obaje, *Geology and mineral resources of Nigeria* Dordtecht, Heidelberg, London, Springer, 2009, pp 218. https://link.springer.com/book/10.1007/978-3-540-92685-6.

[28] I. Garba, ‘‘Geochemical characteristics of mesothermal gold mineralisation in the Pan-African (600 ± 150 Ma) basement of Nigeria", Applied earth sciences (Trans Inst Min Met B) **112** (2003) 319. https://doi.org/10.1179/037174503225003 1.

[29] B. J. Fagbohun, A. O. Ayotunde, A. B. Oluseyi & J. A. Femi, ‘‘Remote detection and interpretation of structural style of the Zuru schist belt, Northwest Nigeria", Geocarto International **37** (2020) 978. https://doi.org/10.1080/10106049.2020.1753822.

[30] Nigerian Geological Survey Agency, *Geological map sheets*, Nigerian Geological Survey Agency, Abuja, Nigeria, 2009, pp. 107-174.

[31] S. Rajagopalan, ‘‘Analytical signal vs reduction to pole: solutions for low magnetic latitudes", Exploration Geo. **34** (2003) 257. https://doi.org/10.1071/EG03257.

[32] A. A. Akinlalu, A. O. Adelusi, G. M. Olayanju, K. A. N. Adiat, G. O. Omosuyi, A. Y. B. Anifowose & B. E. Akeredolu, ‘‘Aeromagnetic mapping of basement structures and mineralization characterization of Ilesa Schist Belt, Southwestern Nigeria", J. African Earth Sci. **138** (2018) 383. https://doi.org/10.1016/j.jafrearsci.2017.11.033.

[33] N. K. Olsunkanmi, O. A. Olufemi, S. Olatunji, N. B. Salawa & B. Toba, ‘‘Interpretation of high resolution aeromagnetic data of Kaoje and its environ, western part of the Zuru Schist belt, Nigeria: implication for Fe–Mn occurrence", Heliyon **6** (2020) e03320. https://doi.org/10.1016/j.heliyon.2020.e03320.

[34] Y. Okubo, R. J. Graf, R. O. Hansen, K. Ogawa & H. Tsu, ‘‘Curie point depths of the island of Kyushu and surrounding area Japan", Geophysics **50** (1985) 481. https://doi.org/10.1190/1.1441926.

[35] C. A. Finn & D. Ravat, ‘‘Magnetic depth estimates and their Potential for constraining crustal composition and heat flow in Antarctica", Eos Transactions American Geophysical Union **85** (2004) T11A. https://www.researchgate.net/publication/241374433_Magnetic_Depth_Estimates_and_Their_Potential_for_Constraining_Crustal_Composition_and_Heat_Flow_in_Antarctica.

[36] A. Stampolidis, I. Kane & G. N. Tsokas, ‘‘Curie point depths of Albania inferred from ground total field magnetic data", Survey Geophysics 26 (2005) 461. https://doi.org/10.1007/s10712-005-7886-2.

[37] N. Maden, ‘‘Curie-point depth from spectral analysis of magnetic data in Erciyes Strato volcano (Central Turkey)", Pure Applied Geophysics 167 (2010) 349. https://doi.org/10.1007/s00024-009-0017-0.

[38] M. Salk, O. Pamukcu & I. Kaftan, ‘‘Determination of Curie point dept and heat flow from magsat data of western Anatolia", Journal of Balkan geophysical society **8** (2005) 149. https://www.researchgate.net/publication/237706743_Determination_of_the_Curie_Point_Depth_and_Heat_Flow_From_Magsat_Data_of_Western_Anatolia.

[39] I. Garba & S. O. Akande, ‘‘The origin and significance of non-aqueous CO2 fluid inclusions in the auriferous veins of Bin Yauri, northwestern Nigeria", Mineral. Deposita **27** (1992) 249. https://doi.org/10.1007/BF00202550.